Characterization of Delay and Doppler Spreads of Underwater Particle Velocity Channels Using Zero Crossing Rates

H. Guo[1], A. Abdi[1], A. Song[2], and M.Badiey[2]

[1] Center for Wireless Communication and Signal Processing Research
Dept. of Electrical and Computer Engineering, New Jersey Institute of Technology, Newark, NJ 07102, USA

[2] Physical Ocean Science and Engineering
College of Earth, Ocean, and Environment, University of Delaware, Newark, DE 19716, USA
Emails: hg45@njit.edu, ali.abdi@njit.edu, ajsong@UDel.edu, badiey@UDel.edu.

***Abstract* —Communication in acoustic particle velocity channel using vector sensors is recently proposed for the underwater medium. Due to the presence of multiple propagation paths, a mobile receiver collects the transmitted signal with different delays and Doppler shifts. This introduces certain delay and Doppler spreads in particle velocity communication channels. In this paper, these channel spreads are characterized using the zero crossing rates of channel responses in frequency and time domain. Useful expressions for delay and Doppler spreads are derived in terms of the key channel parameters, mean angle of arrivals and angle spreads. Closed-form expressions for the temporal correlations of underwater acoustic particle velocity channels are presented as well. These results are needed for design and performance predication of communication systems in time-varying and frequency-selective underwater particle velocity channels.**

I. Introduction

A vector sensor can measure non-scalar components of the acoustic field such as the particle velocity, which cannot be sensed by a single scalar (pressure) sensor. They are mainly used for SONAR and target localization, and have recently been proposed [1][2] and used [3][4] for underwater acoustic communication. Characterization of particle velocity channels and their impact on vector sensor communication systems performance is therefore of interest. In multipath channels such as shallow waters, a vector sensor receives the signal through several paths and each path has a different delay (travel time). Motion of the transmitter or receiver in a multipath channel introduces different Doppler shifts as well. Knowledge of the delay and Doppler spreads in acoustic particle velocity channel is important for efficient design of underwater vector sensor communication system.

It is well known that delay and Doppler spreads are proportional to the zero crossing rates (ZCRs) of the channel in frequency [5][6] and time [7][8] domains, respectively. On the other hand, to calculate the frequency and time domain ZCRs, one needs to obtain the second derivative of corresponding frequency and temporal channel correlations, respectively. So to calculate delay and Doppler spreads in particle velocity channels, expressions for frequency and temporal correlations of such channels should be derived first.

The rest of the paper is organized as follows. Basic formulas and definitions for particle velocity channels are provided in Section II. A statistical model for particle velocity channels sensed by a moving vector sensor array is developed and the frequency and temporal correlation functions are derived in Section III. Using those correlation functions, channel zero crossing rates (ZCRs) are calculated in Section IV. Numerical results are provided in Section V, and concluding remarks are given in Section VI. The Appendix at the end is devoted to the derivation of particle velocity temporal correlations.

This work is supported in part by the National Science Foundation (NSF), Grant CCF-0830190.

II. Definition of Particle Velocity Channels

Vector sensors measure the pressure, as well as the components of the acoustic particle velocity, all in a single point in space. Considering a vector sensor receiver array in a two-dimensional *y*-*z* (range-depth) plane, shown as Fig. 1, there is one pressure sensor transmitter in far field, which is shown as a black sphere, and there are three vector sensor receivers, which are shown as black squares. Each vector sensor measures the pressure, as well as the *y* and *z* components of the particle velocity. This means that there are three pressure channels p, p_1 and p_2, as well as six *pressure-equivalent* velocity channels p^y, p^z, p_1^y, p_1^z, p_2^y and p_2^z, all measured in Pascal (Newton/m^2). In Fig. 1 pressure channels are represented by straight dashed lines, whereas pressure-equivalent velocity channels are shown by curved dashed lines. The velocity channels v^y, v^z, v_1^y, v_1^z, v_2^y and v_2^z are defined according to eq. (1) of [1]. Similarly, pressure-equivalent velocity channels are p^y, p^z, p_1^y, p_1^z, p_2^y and p_2^z, where $p^y=-\rho_0 c v^y$, $p^z=-\rho_0 c v^z$, $p_1^y=-\rho_0 c v_1^y$, $p_1^z=-\rho_0 c v_1^z$, $p_2^y=-\rho_0 c v_2^y$, and $p_2^z=-\rho_0 c v_2^z$ [1]. Here ρ_0 is the density of the fluid and c is the speed of sound.

The received rays at the vector sensor array are shown in Fig. 2, where D_0 is the water depth. Vector sensor 1 is located at $y=L_y/2$ and $z=D-(L_z/2)$, vector sensor 2 is at $y=-L_y/2$ and $z=D+(L_z/2)$ and vector sensor *Rx* is located at $y=0$ and $z=D$. Here, L_y and L_z are the projections of the array length L at *y* and *z* axis, respectively, such that $L=(L_y+L_z)^{1/2}$. All the angles are measured with respect to the positive direction of *y*, counterclockwise. We model the rough sea bottom and its surface as collections of N^b and N^s scatterers, respectively, such that $N^b>>1$ and $N^s>>1$. In this paper, the small letters b and s refer to the bottom and surface, respectively. In Fig. 2, for example, the i-th bottom scatterer is represented by O_i^b, $i=1,2,...,N^b$, whereas O_m^s denotes the m-th surface scatterer, $m=1,2,...,N^s$. Rays scattered from the bottom and the surface toward the vector sensors are shown by solid lines. The rays scattered from O_i^b

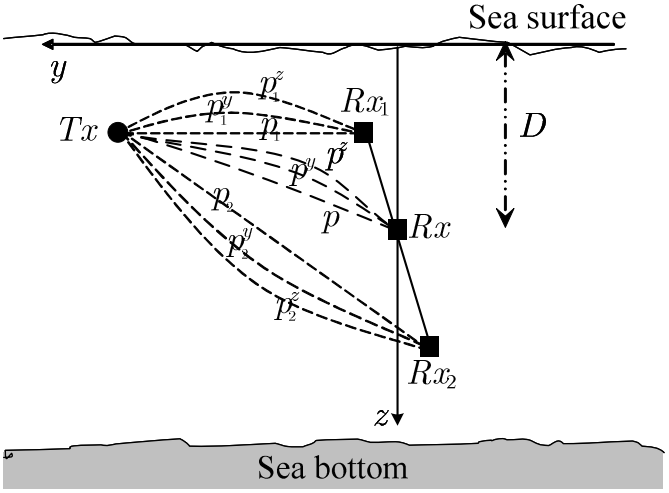

Fig. 1 A system with one pressure transmitter and three vector sensor receivers. Each vector sensor measures the pressure, and the *y* and *z* components of the acoustic particle velocity.

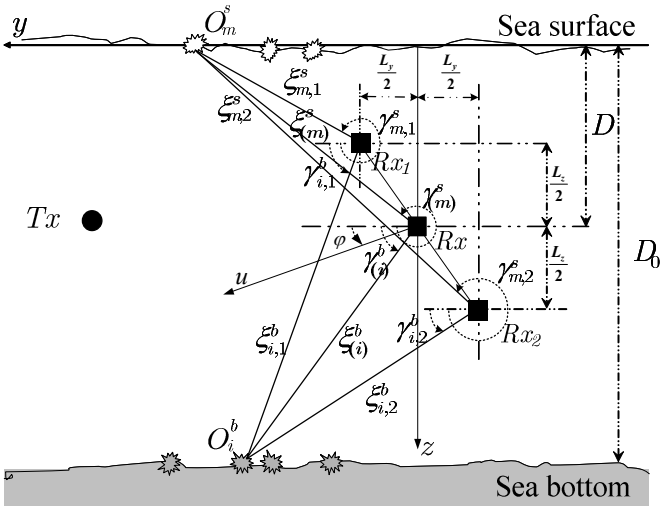

Fig. 2 Received rays at the three vector sensors in a multipath shallow water channel.

hit Rx_1 and Rx_2 at the angle of arrivals (AOAs) $\gamma_{i,1}^b$ and $\gamma_{i,2}^b$, respectively. The traveled distances are labeled by $\xi_{i,1}^b$ and $\xi_{i,2}^b$, respectively. Similarly, the scattered rays from O_m^s impinge Rx_1 and Rx_2 at the AOAs $\gamma_{m,1}^s$ and $\gamma_{m,2}^s$, respectively, with $\xi_{m,1}^s$ and $\xi_{m,2}^s$ as the traveled distances shown in Fig. 2. The vector sensor receivers move at the speed *u*, in the direction specified by φ in Fig. 2.

III. The Correlation Functions

To obtain the channel ZCRs, one needs to derive channel autocorrelations. Similar to [9], for the moving vector sensor array shown in Fig. 2, the pressure channel transfer functions for Rx_1 and Rx_2 can be written as

$$P_1(f,t) = \left(\frac{\Lambda_b}{N^b}\right)^{\frac{1}{2}} \sum_{i=1}^{N^b} \left. \begin{matrix} a_i^b \exp(j\psi_i^b)\exp(-j2\pi f \tau_{i,1}^b) \\ \exp(jk[y\cos(\gamma_{i,1}^b)+z\sin(\gamma_{i,1}^b)]) \\ \exp(j2\pi f_M \cos(\gamma_{i,1}^b-\varphi)t) \end{matrix} \right|_{\substack{y=L_y/2,\\ z=D-L_z/2}}$$
$$+\left(\frac{(1-\Lambda_b)}{N^s}\right)^{\frac{1}{2}} \sum_{m=1}^{N^s} \left. \begin{matrix} a_m^s \exp(j\psi_m^s)\exp(-j2\pi f \tau_{m,1}^s) \\ \exp(jk[y\cos(\gamma_{m,1}^s)+z\sin(\gamma_{m,1}^s)]) \\ \exp(j2\pi f_M \cos(\gamma_{m,1}^s-\varphi)t) \end{matrix} \right|_{\substack{y=L_y/2,\\ z=D-L_z/2}}, \quad (1)$$

$$P_2(f,t) = \left(\frac{\Lambda_b}{N^b}\right)^{\frac{1}{2}} \sum_{i=1}^{N^b} \left. \begin{matrix} a_i^b \exp(j\psi_i^b)\exp(-j2\pi f \tau_{i,2}^b) \\ \exp(jk[y\cos(\gamma_{i,2}^b)+z\sin(\gamma_{i,2}^b)]) \\ \exp(j2\pi f_M \cos(\gamma_{i,2}^b-\varphi)t) \end{matrix} \right|_{\substack{y=-L_y/2,\\ z=D+L_z/2}}$$
$$+\left(\frac{(1-\Lambda_b)}{N^s}\right)^{\frac{1}{2}} \sum_{m=1}^{N^s} \left. \begin{matrix} a_m^s \exp(j\psi_m^s)\exp(-j2\pi f \tau_{m,2}^s) \\ \exp(jk[y\cos(\gamma_{m,2}^s)+z\sin(\gamma_{m,2}^s)]) \\ \exp(j2\pi f_M \cos(\gamma_{m,2}^s-\varphi)t) \end{matrix} \right|_{\substack{y=-L_y/2,\\ z=D+L_z/2}}. \quad (2)$$

In (1) and (2), $a_i^b > 0$ and $a_m^s > 0$ represent the amplitudes of the rays scattered from O_i^b and O_m^s, respectively, whereas $\psi_i^b \in [0, 2\pi)$ and $\psi_m^s \in [0, 2\pi)$ stand for the associated phases. The delays τ in (1) and (2) represent the travel times from the bottom and surface scatterers to the two vector sensors. For example, $\tau_{i,1}^b$ denotes the travel time from O_i^b to Rx_1. Moreover, the AOAs γ stand for the propagation directions of waves scattered from the bottom and surface towards the receivers. For instance, $\gamma_{m,2}^s$ is the AOA of a ray at Rx_2 which is coming from O_m^s. The complex exponential of the form $\exp(jk[y\cos(\gamma)+z\sin(\gamma)])$ in (1) and (2) represent a plane wave with the AOA γ at the point (*y*, *z*), $\exp(-j2\pi f\tau)$ specifies that the plane wave's travel time is τ [9], and $\exp(j2\pi f_M \cos(\gamma-\varphi)t)$ corresponds to its Doppler shift introduced by the motion of the receiver [10][11]. Here $f_M = u/\lambda$ is the maximum Doppler shift. The terms $(N^b)^{-1/2}$ and $(N^s)^{-1/2}$ are included in (1) and (2), to scale the power. Moreover, $0 \le \Lambda_b \le 1$ represents the amount of the contribution of the bottom scatterers, whereas the contribution of the surface scatterers is given by $1-\Lambda_b$.

Based on the definition of the correlation function $C_{P_2P_1}(\Delta f, \Delta t, L_z, L_y) = E[P_2(f+\Delta f, t+\Delta t)P_1^*(f,t)]$, the channel representations in (1) and (2) and following the same approach as [9] and [12], an integral expression can be obtained for the frequency-time-space pressure channel correlation as

$$C_{P_2P_1}(\Delta f, \Delta t, L_z, L_y) = \Lambda_b \int_{\gamma^b=0}^{\pi} \left. \begin{matrix} w^b(\gamma^b)\exp[-jkL_y(\cos(\gamma_2^b)+\cos(\gamma_1^b))/2] \\ \exp[jkD(\sin(\gamma_2^b)-\sin(\gamma_1^b))] \\ \exp[jkL_z(\sin(\gamma_2^b)+\sin(\gamma_1^b))/2] \\ \exp[j2\pi f(\tau_1^b-\tau_2^b)]\exp[-j2\pi\Delta f\tau_2^b] \\ \exp[j2\pi f_M\cos(\gamma^b-\varphi)\Delta t] \end{matrix} \right\} d\gamma^b$$
$$+(1-\Lambda_b)\int_{\gamma^s=\pi}^{2\pi} \left. \begin{matrix} w^s(\gamma^s)\exp[-jkL_y(\cos(\gamma_2^s)+\cos(\gamma_1^s))/2] \\ \exp[jkD(\sin(\gamma_2^s)-\sin(\gamma_1^s))] \\ \exp[jkL_z(\sin(\gamma_2^s)+\sin(\gamma_1^s))/2] \\ \exp[j2\pi f(\tau_1^s-\tau_2^s)]\exp[-j2\pi\Delta f\tau_2^s] \\ \exp[j2\pi f_M\cos(\gamma^s-\varphi)\Delta t] \end{matrix} \right\} d\gamma^s. \quad (3)$$

Here, γ^b and γ^s are the AOAs of rays coming from bottom and surface toward the array center, respectively. The terms $\cos(\gamma_q^b)$, $\cos(\gamma_q^s)$, $\sin(\gamma_q^b)$ and $\sin(\gamma_q^s)$, $q = 1, 2$, represent the corresponding cosine and sine of bottom and surface AOAs for the vector sensors Rx_1 and Rx_2, respectively. Moreover, τ_q^b and τ_q^s, $q = 1, 2$ are travel times from the bottom and surface scatterers to Rx_1 and Rx_2, respectively. Finally, $w^b(\gamma^b)$ and $w^s(\gamma^s)$ in (3) are the probability density functions (PDFs) of the AOAs of the waves coming from the sea bottom and surface, respectively, such that $0 < \gamma^b < \pi$ and $\pi < \gamma^s < 2\pi$. Similar to [9], to obtain pressure-velocity and velocity-velocity channel correlations, one needs to take proper derivatives of the pressure channel correlation in (3).

Now, we focus on the vector sensor receiver *Rx*, to calculate the delay and Doppler spreads of particle velocity channels. With $L_z = L_y = 0$ in (3), it is straight forward to obtain the frequency-time autocorrelation of $P(f,t)$, the time-varying transfer function of the pressure channel, at *Rx* in Fig. 2

$$\begin{aligned} &C_{PP}(\Delta f,\Delta t) \\ &= E[P(f+\Delta f,t+\Delta t)P^*(f,t)] = C_{P_2P_1}(\Delta f,\Delta t,0,0) \\ &= \Lambda_b E_{\gamma^b}\left[\exp[\frac{-j2\pi\Delta f T_b}{\sin(\gamma^b)}]\exp[j2\pi f_M\cos(\gamma^b-\varphi)\Delta t]\right] \\ &+(1-\Lambda_b)E_{\gamma^s}\left[\exp[\frac{-j2\pi\Delta f T_s}{\sin(\gamma^s)}]\exp[j2\pi f_M\cos(\gamma^s-\varphi)\Delta t]\right]. \end{aligned} \tag{4}$$

Here $T_b = (D_0 - D)/c$, the vertical travel time from bottom to *Rx* and $T_s = D/c$, the vertical travel time from surface to *Rx*. Similar to [1] and [2], let us define the time-varying transfer functions for the pressure-equivalent velocity channels at the vector sensor *Rx* as $P^z(f,t) = (jk)^{-1}\partial P(f,t)/\partial z$ and $P^y(f,t) = (jk)^{-1}\partial P(f,t)/\partial y$. Then taking the second derivative of (4) at $L_z = L_y = 0$ provides the following frequency-time autocorrelations of $P^z(f,t)$ and $P^y(f,t)$ at *Rx*, respectively

$$\begin{aligned} &C_{P^zP^z}(\Delta f,\Delta t) = C_{P_2^zP_1^z}(\Delta f,\Delta t,0,0) \\ &= \Lambda_b E_{\gamma^b}\begin{bmatrix}\sin^2(\gamma^b)\exp[\frac{-j2\pi\Delta f T_b}{\sin(\gamma^b)}] \\ \times\exp[j2\pi f_M\cos(\gamma^b-\varphi)\Delta t]\end{bmatrix} \\ &+(1-\Lambda_b)E_{\gamma^s}\begin{bmatrix}\sin^2(\gamma^s)\exp[\frac{-j2\pi\Delta f T_s}{\sin(\gamma^s)}] \\ \times\exp[j2\pi f_M\cos(\gamma^s-\varphi)\Delta t]\end{bmatrix}, \end{aligned} \tag{5}$$

$$\begin{aligned} &C_{P^yP^y}(\Delta f,\Delta t) = C_{P_2^yP_1^y}(\Delta f,\Delta t,0,0) \\ &= \Lambda_b E_{\gamma^b}\begin{bmatrix}\cos^2(\gamma^b)\exp[\frac{-j2\pi\Delta f T_b}{\sin(\gamma^b)}] \\ \times\exp[j2\pi f_M\cos(\gamma^b-\varphi)\Delta t]\end{bmatrix} \\ &+(1-\Lambda_b)E_{\gamma^s}\begin{bmatrix}\cos^2(\gamma^s)\exp[\frac{-j2\pi\Delta f T_s}{\sin(\gamma^s)}] \\ \times\exp[j2\pi f_M\cos(\gamma^s-\varphi)\Delta t]\end{bmatrix}. \end{aligned} \tag{6}$$

Upon setting $\Delta f = 0$ or $\Delta t = 0$ in (4), (5) and (6), one can obtain the temporal or frequency correlations, respectively. Results for spatial and frequency correlations can be found in [9] and [12], whereas temporal correlations are discussed in the Appendix.

IV. ZCRs of Particle Velocity Channels

Let $\alpha(t)$ be a real random process with the temporal autocorrelation $\Gamma_\alpha(\Delta t) = E[\alpha(t+\Delta t)\alpha(t)]$. Then the ZCR of $\alpha(t)$, the average number of times that $\alpha(t)$ crosses the threshold zero per unit time, can be calculated according to [13]

$$n_\alpha^t = \frac{1}{\pi}\sqrt{-\Gamma_\alpha''(\Delta t)\big|_{\Delta t=0}/\Gamma_\alpha(0)}, \tag{7}$$

where double prime is the second derivative. Similarly, if $\alpha(f)$ is a real random process is the frequency domain, then its ZCR, n_α^f, the average number of times that $\alpha(f)$ crosses the threshold zero per unit frequency, is given by

$$n_\alpha^f = \frac{1}{\pi}\sqrt{-\Gamma_\alpha''(\Delta f)\big|_{\Delta f=0}/\Gamma_\alpha(0)}, \tag{8}$$

where $\Gamma_\alpha(\Delta f) = E[\alpha(f+\Delta f)\alpha(f)]$ is the frequency autocorrelation of $\alpha(f)$.

To study the delay and Doppler spreads of particle velocity channels, we need to calculate frequency and time domain ZCRs of the real parts of the complex channels $P^z(f,t)$ and $P^y(f,t)$. To do this, first the autocorrelation of the real part of the pressure channel, $\mathrm{Re}\{P(f,t)\}$, should be determined. Using (4), it is straight forward to obtain

$$\begin{aligned} \Gamma_{\mathrm{Re}\{P\}}(\Delta f,\Delta t) &= E\left[\mathrm{Re}\{P(f+\Delta f,t+\Delta t)\}\,\mathrm{Re}\{P(f,t)\}\right] \\ &= 0.5\,\mathrm{Re}\{C_{PP}(\Delta f,\Delta t)\}. \end{aligned} \tag{9}$$

Similarly, the autocorrelation of the real part of the vertical particle velocity channel, $\mathrm{Re}\{P^z(f,t)\}$, can be written as

$$\begin{aligned} \Gamma_{\mathrm{Re}\{P^z\}}(\Delta f,\Delta t) &= E\left[\mathrm{Re}\{P^z(f+\Delta f,t+\Delta t)\}\,\mathrm{Re}\{P^z(f,t)\}\right] \\ &= 0.5\,\mathrm{Re}\{C_{P^zP^z}(\Delta f,\Delta t)\}. \end{aligned} \tag{10}$$

And the autocorrelation of the real part of the horizontal velocity channel, $\mathrm{Re}\{P^y(f,t)\}$, is given by

$$\begin{aligned} \Gamma_{\mathrm{Re}\{P^y\}}(\Delta f,\Delta t) &= E\left[\mathrm{Re}\{P^y(f+\Delta f,t+\Delta t)\}\,\mathrm{Re}\{P^y(f,t)\}\right] \\ &= 0.5\,\mathrm{Re}\{C_{P^yP^y}(\Delta f,\Delta t)\}. \end{aligned} \tag{11}$$

A. Frequency Domain ZCRs

Here we have $\Delta t = 0$. By inserting (4) into (9), taking derivative with respect to Δf twice and then replacing Δf with zero, for the pressure channel we obtain

$$\begin{aligned} &-\Gamma''_{\mathrm{Re}\{P\}}(\Delta f,0)\big|_{\Delta f=0} = \\ &\Lambda_b 2\pi^2T_b^2E_{\gamma^b}\left[\frac{1}{\sin^2(\gamma^b)}\right]+(1-\Lambda_b)2\pi^2T_s^2E_{\gamma^s}\left[\frac{1}{\sin^2(\gamma^s)}\right]. \end{aligned} \tag{12}$$

Similarly, by inserting (5) into (10) (or (6) into (11)), differentiation with respect to Δf twice and then replacing Δf with zero, for the vertical (or the horizontal) velocity channel we obtain

$$-\Gamma''_{\mathrm{Re}\{P^z\}}(\Delta f,0)\big|_{\Delta f=0} = \Lambda_b 2\pi^2T_b^2 + (1-\Lambda_b)2\pi^2T_s^2, \tag{13}$$

$$\begin{aligned} &-\Gamma''_{\mathrm{Re}\{P^y\}}(\Delta f,0)\big|_{\Delta f=0} = \\ &\Lambda_b 2\pi^2T_b^2E_{\gamma^b}[\frac{\cos^2(\gamma^b)}{\sin^2(\gamma^b)}]+(1-\Lambda_b)2\pi^2T_s^2E_{\gamma^s}[\frac{\cos^2(\gamma^s)}{\sin^2(\gamma^s)}]. \end{aligned} \tag{14}$$

Moreover, by inserting (4) ,(5) and (6) into (9) ,(10) and (11), respectively, it is easy to verify

$$\Gamma_{\mathrm{Re}\{P\}}(0,0)=0.5, \tag{15}$$

$$\Gamma_{\mathrm{Re}\{P^z\}}(0,0)=\frac{\Lambda_b}{2}E_{\gamma^b}\left[\sin^2(\gamma^b)\right]+\frac{(1-\Lambda_b)}{2}E_{\gamma^s}\left[\sin^2(\gamma^s)\right], \tag{16}$$

$$\Gamma_{\mathrm{Re}\{P^y\}}(0,0)=\frac{\Lambda_b}{2}E_{\gamma^b}\left[\cos^2(\gamma^b)\right]+\frac{(1-\Lambda_b)}{2}E_{\gamma^s}\left[\cos^2(\gamma^s)\right]. \tag{17}$$

To obtain $n^f_{\mathrm{Re}\{P\}}$, $n^f_{\mathrm{Re}\{P^z\}}$ and $n^f_{\mathrm{Re}\{P^y\}}$, frequency domain ZCRs, one needs to simply divide (12), (13) and (14) by (15), (16) and (17), respectively.

B. Time Domain ZCRs

Now we have $\Delta f=0$. Similarly to the previous frequency domain derivations, we can obtain the following results in time domain

$$\begin{aligned}-\Gamma''_{\mathrm{Re}\{P\}}(0,\Delta t)\big|_{\Delta t=0}&=\Lambda_b 2\pi^2 f_M^2 E_{\gamma^b}\left[\cos^2(\gamma^b-\varphi)\right]\\&\quad+(1-\Lambda_b)2\pi^2 f_M^2 E_{\gamma^s}\left[\cos^2(\gamma^s-\varphi)\right],\end{aligned} \tag{18}$$

$$\begin{aligned}-\Gamma''_{\mathrm{Re}\{P^z\}}(0,\Delta t)\big|_{\Delta t=0}&=\Lambda_b 2\pi^2 f_M^2 E_{\gamma^b}\left[\sin^2(\gamma^b)\cos^2(\gamma^b-\varphi)\right]\\&\quad+(1-\Lambda_b)2\pi^2 f_M^2 E_{\gamma^s}\left[\sin^2(\gamma^s)\cos^2(\gamma^s-\varphi)\right],\end{aligned} \tag{19}$$

$$\begin{aligned}-\Gamma''_{\mathrm{Re}\{P^y\}}(0,\Delta t)\big|_{\Delta t=0}&=\Lambda_b 2\pi^2 f_M^2 E_{\gamma^b}\left[\cos^2(\gamma^b)\cos^2(\gamma^b-\varphi)\right]\\&\quad+(1-\Lambda_b)2\pi^2 f_M^2 E_{\gamma^s}\left[\cos^2(\gamma^s)\cos^2(\gamma^s-\varphi)\right].\end{aligned} \tag{20}$$

By dividing (18), (19) and (20) by (15), (16) and (17), respectively, time domain ZCRs $n^t_{\mathrm{Re}\{P\}}$, $n^t_{\mathrm{Re}\{P^z\}}$ and $n^t_{\mathrm{Re}\{P^y\}}$ will be obtained.

V. Numerical Results

Equations (12) - (20), which determine ZCR and therefore delay and Doppler spreads, are valid for any AOA distribution model. Here we use the Gaussian PDF, eq. (28) in [9], to model the AOAs. Gaussian PDFs are particularly useful when angle spreads are small. For large angle spreads, one can use the von Mises PDF [14].

For Gaussian AOA PDFs with small angle spreads, mathematical expectations in (12) - (20) can be calculated in closed-forms, using the Taylor series expansions of γ^b and γ^s around mean AOA μ_b and μ_s, respectively. For example

$$\begin{aligned}\frac{1}{\sin^2(\gamma^b)}&\approx\csc^2(\mu_b)-2\csc^2(\mu_b)\cot(\mu_b)(\gamma^b-\mu_b)\\&\quad+\left(\cos(2\mu_b)+2\right)\csc^4(\mu_b)(\gamma^b-\mu_b)^2,\end{aligned} \tag{21}$$

where $\csc(\cdot)=1/\sin(\cdot)$ and $\cot(\cdot)=\cos(\cdot)/\sin(\cdot)$. Other sin and cos terms in (12) - (20) can be represented by Taylor series as well. Clearly, similar results can be obtained for γ^s, in terms of μ_s and σ_s.

To obtain some insight, we consider a case where the bottom components are dominate, i.e., $\Lambda_b=1$. Then we provide closed-form frequency and time domain ZCRs in the following subsections.

A. Frequency Domain ZCRs

By inserting (12) - (17) into the ZCR formula in (8) and using the Taylor series, one can show that

$$n^f_{\mathrm{Re}\{P\}}=2T_b\left[\csc^2(\mu_b)+\left(\cos(2\mu_b)+2\right)\csc^4(\mu_b)\sigma_b^2\right]^{\frac{1}{2}}, \tag{22}$$

$$n^f_{\mathrm{Re}\{P^z\}}=2T_b\left[1/\left(\sin^2(\mu_b)+\cos(2\mu_b)\sigma_b^2\right)\right]^{\frac{1}{2}}, \tag{23}$$

$$n^f_{\mathrm{Re}\{P^y\}}=2T_b\left[\frac{\cot^2(\mu_b)+\left(\cos(2\mu_b)+2\right)\csc^4(\mu_b)\sigma_b^2}{\cos^2(\mu_b)-\cos(2\mu_b)\sigma_b^2}\right]^{\frac{1}{2}}. \tag{24}$$

Equations (22) - (24), normalized by T_b, are plotted in Fig. 3. Simulation results are also included, which show the accuracy of derived formulas.

Fig. 3 shows the dependence of frequency domain ZCRs on the angle spread. As expected, the ZCRs of *y*-velocity and pressure channels are very close. This is because the waves are coming through an almost horizontal direction ($\mu_b=5$). Increase of ZCRs with the angle spread can be related to the fact that as the angle spread increases, more rays from different directions reach the receiver. This means larger delay spreads, which results in large ZCRs in the frequency domain. Since in the case considered in Fig. 3, most of the angle of arrivals are horizontal, the coming rays do not contribute much to the *z*-velocity channel. This explains the lower values of the frequency domain *z*-velocity ZCR. This can be better understood by comparing the impulse responses of particle velocity and pressure channels in Fig. 4. This figure is obtained by plotting the impulse response in eq. (6) of [9], and its derivatives with respect to *y* and *z*, for $\mu_b=5^\circ$ and $\sigma_b=3^\circ$. Clearly the impulse response of the *z* channel is spread over a small range of delays in this example. These are consistent with the delay spread results in [12], obtained via a different approach. The advantage of the proposed velocity channel delay spread analysis here via frequency domain ZCR is that it provides analytical expressions such as (23) and (24). These types of expressions quantify the delay spreads of acoustic particle velocity and pressure channels in terms of key channel parameters such as mean angle of arrivals and angle spreads.

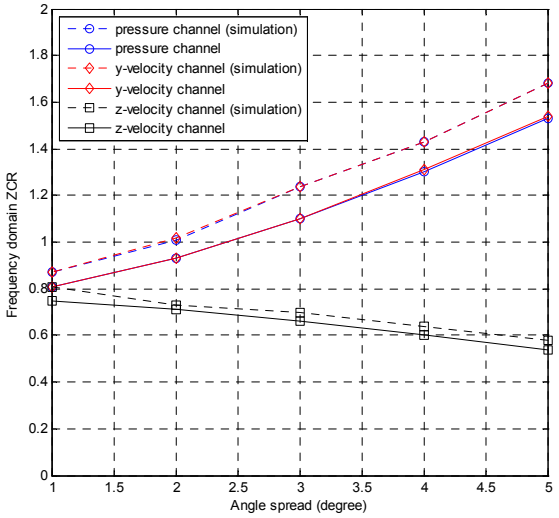

Fig. 3 Frequency-domain zero crossing rates of particle velocity and pressure channels versus the angle spread σ_b ($\mu_b=5^\circ$).

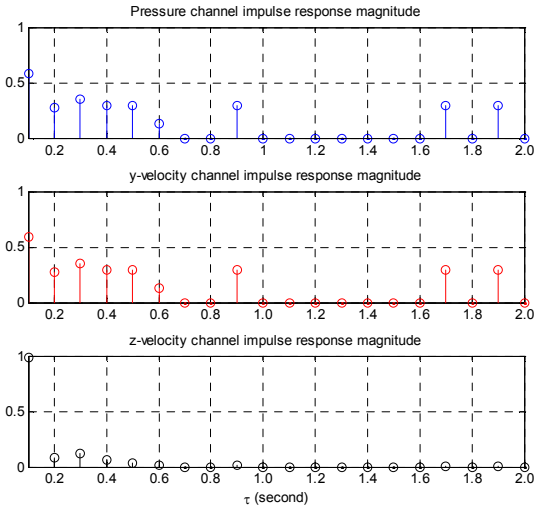

Fig. 4 Normalized impulse responses of particle velocity and pressure channels.

B. *Time Domain ZCRs*

By inserting (18) - (20) and (15) - (17) into the ZCR formula in (7), and using the Taylor series as well, the following results can be obtained

$$n^t_{\mathrm{Re}\{P\}} = 2f_M\left[\cos^2(\mu_b-\varphi)+\cos(2\mu_b-2\varphi)\sigma_b^2\right]^{\frac{1}{2}}, \quad (25)$$

$$n^t_{\mathrm{Re}\{P^z\}} = 2f_M\frac{\left[\begin{array}{l}\cos^2(\mu_b-\varphi)\sin^2(\mu_b)\\ +0.5(\cos(2\mu_b)+2\cos(4\mu_b-2\varphi)-\cos(2\mu_b-2\varphi))\sigma_b^2\end{array}\right]^{\frac{1}{2}}}{\left[\sin^2(\mu_b)+\cos(2\mu_b)\sigma_b^2\right]^{\frac{1}{2}}}, \quad (26)$$

$$n^t_{\mathrm{Re}\{P^y\}} = 2f_M\frac{\left[\begin{array}{l}\cos^2(\mu_b)\cos^2(\mu_b-\varphi)\\ -0.5(\cos(2\mu_b)+2\cos(4\mu_b-2\varphi)+\cos(2\mu_b-2\varphi))\sigma_b^2\end{array}\right]^{\frac{1}{2}}}{\left[\cos^2(\mu_b)-\cos(2\mu_b)\sigma_b^2\right]^{\frac{1}{2}}}. \quad (27)$$

Equations (25) - (27), normalized by f_M are plotted in Fig. 5, along with simulation results, which demonstrate the accuracy of the analytical results. According to this figure, time domain ZCRs of particle velocity and pressure channels are about the same, and not dependent much on the angle spread, for the case considered.

VI. Conclusion

In this paper, the delay and Doppler spreads of particle velocity channels are studied. A zero crossing framework is developed to study delay and Doppler spreads in multipath underwater acoustic particle velocity and pressure channels. Using the channel correlation functions, delay and Doppler spreads are calculated by deriving closed-form expressions for channel zero-crossing rates in frequency and time, respectively. These expressions show how particle velocity channel delay and Doppler spreads may depend on some key parameters of the channel such as mean angle of arrival and angle spread. The results are useful for design and performance predication of vector sensor communication systems that operate in time-varying and frequency-selective acoustic particle velocity channels.

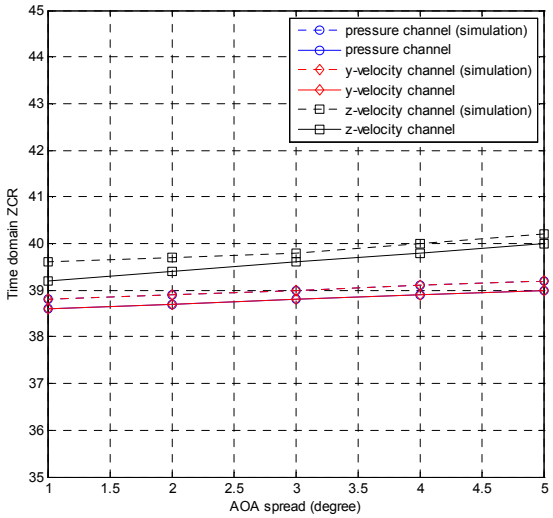

Fig. 5 Time-domain zero crossing rates of particle velocity and pressure channels versus the angle spread σ_b ($\mu_b = 5^\circ$, $\varphi = 0^\circ$).

Appendix.
Temporal Correlations in Particle Velocity Channels

As discussed in Section III, with $\Delta f = L_y = L_z = 0$ in eq. (3) or (4), one obtains the pressure channel temporal correlation at the point *Rx* in Fig. 2

$$\begin{aligned} C_{PP}(0,\Delta t) &= E[P(f,t+\Delta t)P^*(f,t)] \\ &= \Lambda_b \int_{\gamma^b=0}^{\pi} w^b(\gamma^b)\exp[j2\pi f_M\cos(\gamma^b-\varphi)\Delta t]d\gamma^b \\ &\quad +(1-\Lambda_b)\int_{\gamma^s=\pi}^{2\pi} w^s(\gamma^s)\exp[j2\pi f_M\cos(\gamma^s-\varphi)\Delta t]d\gamma^s. \end{aligned} \quad (28)$$

$\Delta f = 0$ in (5) and (6) results in particle velocity temporal correlation at *Rx* in Fig. 2

$$\begin{aligned} C_{P^zP^z}(0,\Delta t) &= E[P^z(f,t+\Delta t)\{P^z(f,t)\}^*] \\ &= \Lambda_b \int_{\gamma^b=0}^{\pi} w^b(\gamma^b)\sin^2(\gamma^b)\exp[j2\pi f_M\cos(\gamma^b-\varphi)\Delta t]d\gamma^b \\ &\quad +(1-\Lambda_b)\int_{\gamma^s=\pi}^{2\pi} w^s(\gamma^s)\sin^2(\gamma^s)\exp[j2\pi f_M\cos(\gamma^s-\varphi)\Delta t]d\gamma^s, \end{aligned} \quad (29)$$

$$\begin{aligned} C_{P^yP^y}(0,\Delta t) &= E[P^y(f,t+\Delta t)\{P^y(f,t)\}^*] \\ &= \Lambda_b \int_{\gamma^b=0}^{\pi} w^b(\gamma^b)\cos^2(\gamma^b)\exp[j2\pi f_M\cos(\gamma^b-\varphi)\Delta t]d\gamma^b \\ &\quad +(1-\Lambda_b)\int_{\gamma^s=\pi}^{2\pi} w^s(\gamma^s)\cos^2(\gamma^s)\exp[j2\pi f_M\cos(\gamma^s-\varphi)\Delta t]d\gamma^s. \end{aligned} \quad (30)$$

Now we consider small AOA spreads, with Gaussian distributions and Taylor series for sin and cos [9]. Using the characteristic function of a Gaussian random variable utilized in [9] to calculate integrals similar to those in (28) - (30), the following closed-form temporal correlations can be obtained

$$\begin{aligned} C_{PP}(0,\Delta t) &= \Lambda_b \exp[j2\pi f_M \Delta t \cos(\mu_b - \varphi)] \\ &\times \exp[-2\sigma_b^2 \pi^2 f_M^2 \Delta t^2 \sin^2(\mu_b - \varphi)] \\ &+ (1-\Lambda_b)\exp[j2\pi f_M \Delta t \cos(\mu_s - \varphi)] \\ &\times \exp[-2\sigma_s^2 \pi^2 f_M^2 \Delta t^2 \sin^2(\mu_s - \varphi)], \end{aligned} \tag{31}$$

$$\begin{aligned} C_{P^z P^z}(0,\Delta t) = \Lambda_b & \begin{bmatrix} \sin^2(\mu_b) - \sigma_b^2 \cos^2(\mu_b) \\ +4\pi f_M \Delta t \sigma_b^2 \cos(\mu_b)\sin(\mu_b)\sin(\mu_b - \varphi) \\ +4\pi^2 f_M^2 \Delta t^2 \sigma_b^4 \cos^2(\mu_b)\sin^2(\mu_b - \varphi) \end{bmatrix} \\ \times \exp & \begin{bmatrix} j2\pi f_M \Delta t \cos(\mu_b - \varphi) \\ -2\sigma_b^2 \pi^2 f_M^2 \Delta t^2 \sin^2(\mu_b - \varphi) \end{bmatrix} \\ + (1-\Lambda_b) & \begin{bmatrix} \sin^2(\mu_s) - \sigma_s^2 \cos^2(\mu_s) \\ +4\pi f_M \Delta t \sigma_s^2 \cos(\mu_s)\sin(\mu_s)\sin(\mu_s - \varphi) \\ +4\pi^2 f_M^2 \Delta t^2 \sigma_s^4 \cos^2(\mu_s)\sin^2(\mu_s - \varphi) \end{bmatrix} \\ \times \exp & \begin{bmatrix} j2\pi f_M \Delta t \cos(\mu_s - \varphi) \\ -2\sigma_s^2 \pi^2 f_M^2 \Delta t^2 \sin^2(\mu_s - \varphi) \end{bmatrix}, \end{aligned} \tag{32}$$

$$\begin{aligned} C_{P^y P^y}(0,\Delta t) = \Lambda_b & \begin{bmatrix} \cos^2(\mu_b) - \sigma_b^2 \sin^2(\mu_b) \\ -4\pi f_M \Delta t \sigma_b^2 \cos(\mu_b)\sin(\mu_b)\sin(\mu_b - \varphi) \\ +4\pi^2 f_M^2 \Delta t^2 \sigma_b^4 \sin^2(\mu_b)\sin^2(\mu_b - \varphi) \end{bmatrix} \\ \times \exp & \begin{bmatrix} j2\pi f_M \Delta t \cos(\mu_b - \varphi) \\ -2\sigma_b^2 \pi^2 f_M^2 \Delta t^2 \sin^2(\mu_b - \varphi) \end{bmatrix} \\ + (1-\Lambda_b) & \begin{bmatrix} \cos^2(\mu_s) - \sigma_s^2 \sin^2(\mu_s) \\ -4\pi f_M \Delta t \sigma_s^2 \cos(\mu_s)\sin(\mu_s)\sin(\mu_s - \varphi) \\ +4\pi^2 f_M^2 \Delta t^2 \sigma_s^4 \sin^2(\mu_s)\sin^2(\mu_s - \varphi) \end{bmatrix} \\ \times \exp & \begin{bmatrix} j2\pi f_M \Delta t \cos(\mu_s - \varphi) \\ -2\sigma_s^2 \pi^2 f_M^2 \Delta t^2 \sin^2(\mu_s - \varphi) \end{bmatrix}. \end{aligned} \tag{33}$$

Analytical temporal correlations in (31) - (33) are plotted in Fig. 6 for $\varphi = 0^\circ$ and $u = 2.5m/s$. Simulation results are also provided to verify analytical expressions. Note that as discussed in [9], the average pressure channel power is equal to the sum of the average powers of z and y particle velocity channels. This can also be observed here by having $\Delta t = 0$ in (28) - (30), or (31) - (33) or in Fig. 6.

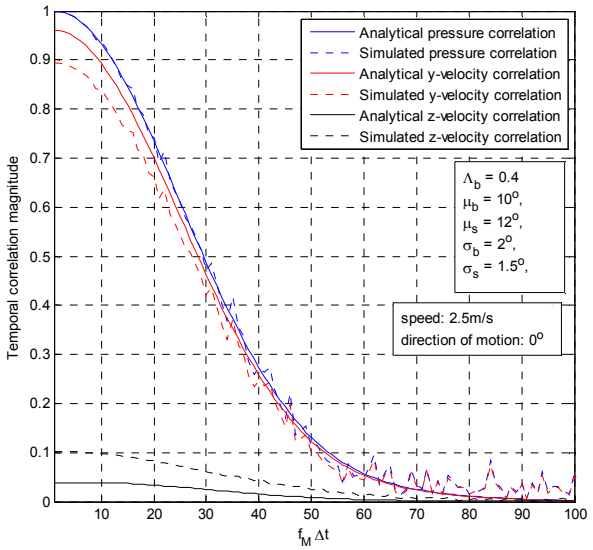

Fig. 6 Temporal correlation of the pressure channel, as well as horizontal and vertical particle velocity channels.

REFERENCES

[1] A. Abdi and H. Guo, "A new compact multichannel receiver for underwater wireless communication networks," *IEEE Trans. Wireless Commun.*, vol. 8, pp. 3326-3329, 2009.

[2] A. Abdi, H. Guo and P. Sutthiwan, "A new vector sensor receiver for underwater acoustic communication," in *Proc. MTS/IEEE Oceans*, Vancouver, BC, Canada, 2007.

[3] H. Guo and A. Abdi, "Multiuser underwater communication with space-time block codes and acoustic vector sensors," in *Proc. MTS/IEEE Oceans*, Quebec City, QC, Canada, 2008.

[4] A. Song, M. Badiey, P. Hursky and A. Abdi, "Time reversal receivers for underwater acoustic communication using vector sensors," in *Proc. MTS/IEEE Oceans*, Quebec City, QC, Canada, 2008.

[5] K. Witrisal, "On estimating the RMS delay spread from the frequency-domain level crossing rate," *IEEE Commun. Lett.*, vol. 5, pp. 287-289, 2001.

[6] K. Witrisal, Y. Kim and R. Prasad, "A new method to measure parameters of frequency-selective radio channels using power measurements," *IEEE Trans. Commun.*, vol. 49, pp. 1788-1800, 2001.

[7] H. Zhang and A. Abdi, "On the average crossing rates in selection diversity," *IEEE Trans. Wireless Commun.*, vol. 6, pp. 448-451, 2007.

[8] N. C. Beaulieu and X. Dong. "Level crossing rate and average fade duration of MRC and EGC diversity in Ricean fading," *IEEE Trans. Commun*, vol. 51, pp. 722-726, 2003.

[9] A. Abdi and H. Guo, "Signal correlation modeling in acoustic vector sensor arrays," *IEEE Trans. Signal Processing*, vol. 57, pp. 892-903, 2009.

[10] A. Abdi and M. Kaveh, "Parametric modeling and estimation of the spatial characteristics of a source with local scattering," in *Proc. IEEE Int. Conf. Acoust., Speech, Signal Processing*, Orlando, FL, 2002, pp. 2821-2824.

[11] C. Bjerrum-Niese, L. Bjorno, M. A. Pinto and B. Quellec, "A simulation tool for high data-rate acoustic communication in a shallow-water, time-varying channel," *IEEE J. Ocean. Eng.*, vol. 21, pp143-149, 1996.

[12] H. Guo, A. Abdi, A. Song and M. Badiey., "Correlations for underwater acoustic particle velocity and pressure channels," in *Proc. Conf. Inform. Sci. Syst.*, Johns Hopkins University, Baltimore, MD, 2009, pp. 913-918.

[13] A. Papoulis, *Probability, Random Variables, and Stochastic Processes*, 3rd ed., Singapore: McGraw-Hill, 1991.

[14] A. Abdi, J. A. Barger and M. Kaveh, "A parametric model for the distribution of the angle of arrival and the associated correlation function and power spectrum at the mobile station," *IEEE Trans. Veh. Technol.* vol. 51, pp.425-434, 2002.